TECHNICAL ARTICLE

Microstructural Analysis of Ballistic Tests on Welded Armor Steel Joints

**M. Balakrishnan · V. Balasubramanian ·
G. Madhusudhan Reddy**

Abstract The deformation and fracture behavior of welded joints made from quenched and tempered steel closely conforming to AISI 4340 were investigated. Due to weld thermal cycles and under matching fillers, the welded armor steel joints showed poor ballistic performance compared with the base metal (BM). The problems encountered in the past were reduced by depositing a soft austenitic stainless-steel buttering layer in between the BM and the hardfaced layer. This method showed enhancement in ballistic performance and good weld integrity. In this investigation, an attempt is made to investigate the microstructure after ballistic testing on the weld metal zone consisting of the hardfaced interlayer. The results reveal the microstructural characteristics before and after ballistic testing of armor steel welds fabricated using the shielded metal arc welding (SMAW) process.

Keywords Welding · Hardfacing · Sandwich structures · Ballistic impact · Microstructures

M. Balakrishnan · V. Balasubramanian (✉)
Center for Materials Joining & Research (CEMAJOR),
Department of Manufacturing Engineering, Annamalai University, Annamalai Nagar 608 002, Tamil Nadu, India
e-mail: visvabalu@yahoo.com

G. Madhusudhan Reddy
Solidification Technology Division, Metal Joining Group,
Defense Metallurgical Research Laboratory (DMRL),
Kanchanbagh, Hyderabad 500058, India

Introduction

Armor-grade quenched and tempered (Q&T) steel is used for protection of military and nonmilitary vehicles, because of its high energy-absorbing properties. Q&T steels used for armor applications require high strength, notch toughness, and hardness [1–3]. Most of the research carried out in the past on Q&T armor steel has concentrated on hydrogen-induced cracking (HIC) [4–6], heat-affected zone (HAZ) softening [7–9], ceramic front layer and metallic back layer composites, or fiber-encapsulated composites [10]. It was recently reported that the presence of an austenitic stainless-steel (SS) buttering layer between the armor plate [base metal (BM)] and weld metal/hardfaced metal resulted in enhanced ballistic performance and successfully held the weld layers intact when a projectile was fired at interfaces and the heat-affected zone (HAZ) [11]. It was also reported that the ballistic performance of the weld metal is enhanced, resulting in shattering of the projectile [12].

High-strain-rate fracture and failure of a high-strength low-alloy steel in compression were investigated by Odeshi et al. [13]. It was observed that thermal softening as a result of adiabatic heating in the materials controls the deformation and fracture behavior. The role of retained austenite, twinned plate martensite interfaces, and grain boundaries in determining the ballistic performance of steel was explored by Maweja and Stumpf [14]. The effect of the target plate's strength on the perforation of steel plates was also studied by Deya et al. [15]. The experimental results indicated that, for perforation by blunt projectiles, the ballistic limit velocity decreased with increasing strength, while the opposite trend was found in tests with conical and ogival projectiles. The structure, dislocation substructure, and mechanical properties of targets made of four

aluminum alloys after impact loading by a kinetic energy projectile were investigated by Milman et al. [16]. Murr et al. [17] explored the novel deformation processes, microstructures involving ballistic penetrator formation, hypervelocity impact, and penetration phenomena using light and transmission electron microscopy. From this literature review, it is apparent that the reported work on the microstructural characteristics of ballistic tested weld metal region is very scant. Hence, this investigation aims to evaluate the microstructural features of ballistic tested armor steel welds (before and after ballistic testing) in continuation of the study reported by Balakrishnan et al. [12]. This article reports the changes observed in the microstructural features along the projectile trajectory in a multilayered armor steel joint after ballistic testing.

Experimental Work

The BM used in this study was 18-mm-thick high-strength, low-alloy Q&T steel closely conforming to the AISI 4340 specification. Heat treatment applied to the BM consisted of austenizing at 900 °C followed by oil quenching and subsequent tempering at 250 °C. This heat treatment yields high hardness and strength, and good toughness for this BM. The chemical compositions of BM and filler metal are presented in Table 1. In this investigation, an unequal double V-joint configuration was prepared as shown in Fig. 1. The beveled edges were buttered with SS electrodes and hardfaced with 5.5-mm-thick chromium carbide; the result was a hardfaced interlayer between SS root and capping weld layers. The specifics of the buttering procedure are discussed elsewhere [11, 12]. The shielded metal arc welding (SMAW) process was selected because it is commonly employed in the fabrication of combat vehicles [18]. The SS electrode was selected because it avoids the time-delayed cracking tendency of Q&T steel weldments [3]. The preheating and interpass temperatures were maintained at 150 °C during welding. The fabricated target was subjected to standard ballistic testing, and its performance was compared with that of the armor-grade Q&T steel BM. The ballistic test procedure was discussed in previous publications [2, 7, 8, 10–12]. Four shots were fired into the welded target plate to evaluate its ballistic performance. The depth of penetration (DOP) of the projectile into the target plate was the metric used for evaluating ballistic performance. The weldment was characterized by microstructural analysis and hardness measurements. Etchants used included 2 % Nital for BM and HAZ region, aqua regia for the SS weld metal region, and Vilella's reagent for the hardfaced region. After ballistic testing, the weld metal region (where the projectile impacted) was

carefully extracted in the through-thickness direction for analysis via light microscopy. Hardness measurements were carried out as per the ASTM E-384-05 standard [19] before and after ballistic testing. A Vickers microhardness testing machine was employed to measure the hardness along the weld center line (WCL) and across the WCL with 500 g load for dwell time of 15 s. X-ray diffraction (XRD) patterns were obtained from sections containing only BM and sections containing both weld metal (SS root, hardfaced middle layer, and SS capping) and BM. The fracture surfaces of impacted targets were analyzed by scanning electron microscopy (SEM).

Results

Ballistic Performance

The ballistic test results are presented in Table 2. In all four locations, namely fusion line (FL), WCL, HAZ, and BM, the target offers maximum resistance and thus successfully stopped the projectiles. Of the four locations, the WCL offers the highest resistance compared with other locations (DOP of only 14 mm).

Microstructure

Light micrographs of various locations before ballistic testing are shown in Fig. 2. The microstructure of the BM (Fig. 2a) consists of acicular martensite with fine needles of lath martensite, in addition to some retained austenite [20]. The image analysis result revealed the presence of 97.2 % martensite and 2.7 % retained austenite in the BM microstructure. The microstructures of various locations of the multilayered joint are presented in Fig. 2(b–i). The undiluted weld metal microstructure in the SS buttering and SS capping (Fig. 2b) contains grain boundary δ-ferrite in a plain austenitic matrix. The weld interface (IF) region of the SS buttering and BM (Fig. 2c) contains a continuous epitaxial growth of austenite. The weld interface region of hardfacing and SS capping (Fig. 2d) shows an epitaxial growth of δ-ferrite in austenitic matrix. Figure 2(e) presents the macrostructure of the welded joint and shows the different layers/regions of the joint. From this macrograph, it is clear that the joint has very good integrity and complete fusion at all interfaces was achieved. The HAZ is also visible in the macrostructure. The undiluted hardfaced region (Fig. 2f) contains homogeneous cast-like structure and is composed of hard phase precipitates of hexagonal chromium carbides of different sizes on softer austenitic matrix [21]. Large spine-like

Table 1 Chemical composition (wt.%) of base metal and all weld metal deposits

Element	C	Mn	Si	S	P	Cr	Ni	Mo	V	Fe
Base metal (AISI 4340)	0.35	0.54	–	–	–	1.25	1.75	0.52	–	Bal
ASS electrode (AWS E 307-16)	0.08	3.3	0.90	0.015	0.04	20.30	8.50	1.5	–	Bal
Hardfacing alloy (AWS E FeCr-A7)	4.0	1.0	1.50	–	–	30.00	–	2.0	0.50	Bal

Fig. 1 Joint configuration

a Joint

b Section at A-A

All dimensions are in mm
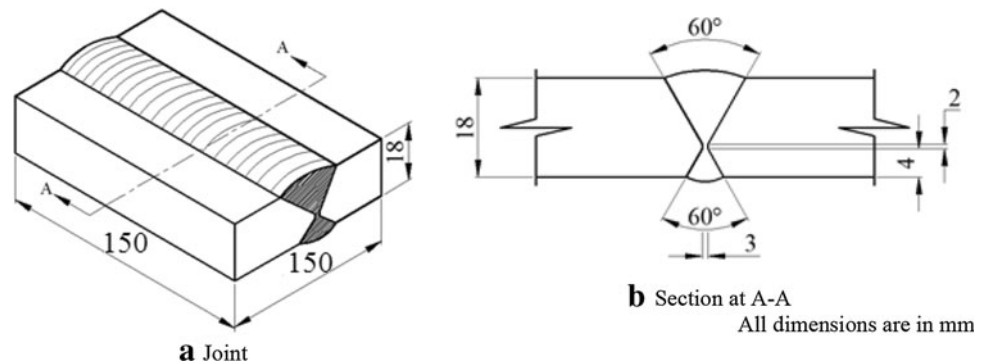
Table 2 Ballistic test results

Shot number	Velocity of projectile (m/s)	Location of projectile impact on target	Failure type	Depth of penetration into the target (mm)	Illustration
1	826.31	Fusion line	S1[a]	16	Stopped
2	832.81	Weld	S1[a]	14	Stopped
3	827.40	Base metal	S2[b]	16	Stopped
4	827.82	HAZ	S1[a]	17	Stopped

[a] No bulge

[b] Smooth bulge

carbides are clearly visible in the microstructure of the hardfaced layers in the joints. The HAZ microstructure (Fig. 2g) clearly depicts the presence of coarse martensite near the FL and toward the BM side; it contains uniformly distributed martensite along with low-temperature products such as bainite [22]. The weld interface region of SS buttering and hardfacing (Fig. 2h) reveals fine continuous epitaxial growth of austenitic matrix and hexagonal carbides. The interface region between buttering layer and BM, and between buttering layers and hardfacing, has similar morphology. The interface microstructure of the sandwiched joint has a smaller portion of unmixed zone near to the periphery of the fusion boundary along with a softened layer of untempered martensite structure. Figure 2(i) shows the SS root microstructure, which clearly depicts the presence of vermicular δ-ferrite dispersed in a massive austenite matrix.

Figure 3 shows the microstructure of the material surrounding the projectile path in the through-thickness direction of the target plate at the WCL location. Microstructural features of encircled locations are discussed in the following paragraphs.

Figure 4(a, b) shows the microstructural features of location "A" at different magnifications. This location corresponds to the interface between the BM and SS buttering layer. Figure 4(a) reveals a number of small fragmentations of the layer. Though it is disintegrated into a number of pieces, in the middle (Fig. 4a) there is a part which shows the integrity of the fusion between buttering layer and hardfaced layer. The micrograph clearly shows that the crack exists only in the high-hardness hardfaced layer and in the low-hardness buttering layer, but not in the interface between the buttering layer and BM. This suggests that the joint integrity is enhanced by the buttering layer. A blunted crack at the interface between SS buttering and hardfacing is visible in Fig. 4(b). In the same micrograph, the hardfaced layer consists of a number of microcracks. At higher magnification, the interface region between SS buttering layer and hardfacing layer shows few microvoids (Fig. 4b). Figure 4(b) reveals the presence of a number of very fine microcracks in the SS buttering layer also. However, good bonding between hardfaced layer and buttering layer is clearly visible in the same micrograph. This suggests that the soft and tough buttering layer was
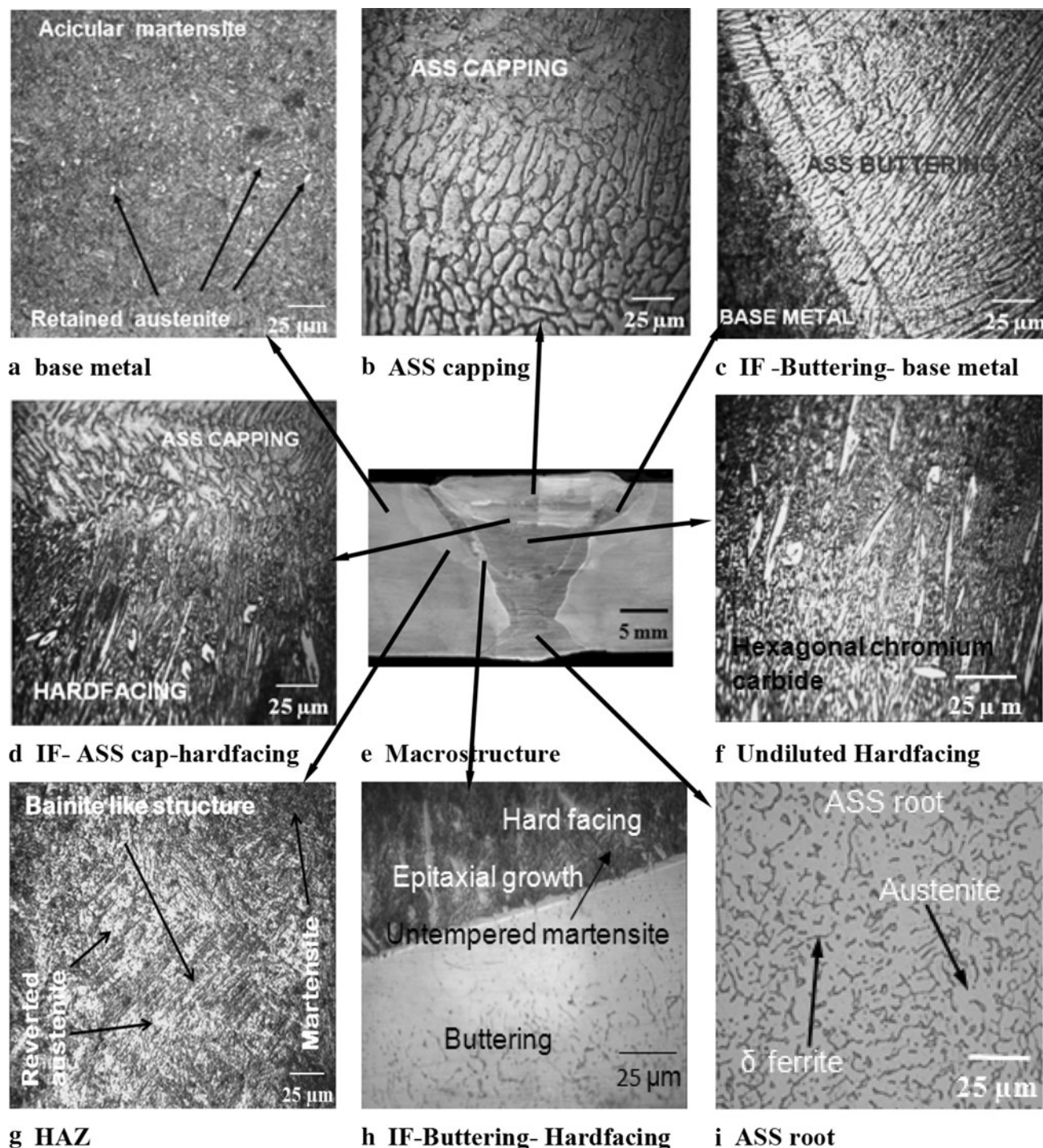
Fig. 2 Optical micrographs of BM and weld metal at various locations

able to absorb some of the impact energy by cracking on its own in the presence of the hardfaced layer.

Figure 5 shows the microstructure after ballistic impact at location "B" in Fig. 3. Figure 5(a) shows the presence of cracks in the hardfaced layer both parallel and normal to the bullet trajectory. When the projectile hits the hard layer directly, it proceeds off-beam and tends to produce more

cracks in the hard layer [23]. This might lead to fragmentation and separation from the subsequent layers. These cracks presented in the hardfaced layer are arrested at the interface between the hardfacing and buttering layer, and this is clearly visible in Fig. 5(a). At the interface between the buttering layer and hardfacing layer (Fig. 5a), the presence of some small microvoids is clearly visible.

These microvoids are not presented in the direction parallel to the bullet trajectory. This suggests that the separation of buttering layer and hardfacing layer after impact is still prevented due to the presence of the soft austenitic buttering layer. Cracks both parallel and normal to the direction of the projectile trajectory are clearly visible in Fig. 5(b). In the same microstructure, the presence of hexagonal chromium carbides is also observed.

Figure 5(b) reveals the presence of transgranular failure of hexagonal chromium carbides in the horizontal crack path. In addition, the presence of gross plastic deformation (elongated chromium carbide) is also observed in the same figure (Fig. 5c). Figure 5(c) reveals the crack path, which shows transgranular failure of high-hardness hexagonal chromium carbide. The hard layer of high-carbon, high-chromium carbide alloy absorbs the ballistic impact energy by forming high-density cracks. The distribution and shape of these cracks seem to be dependent on the distance from
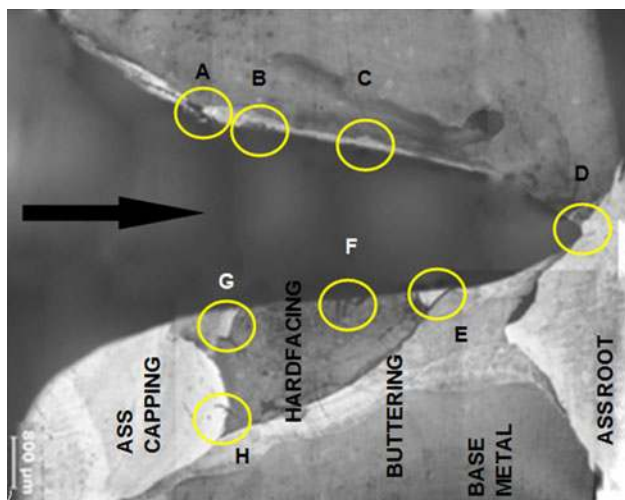
the impact point. They vary in amount from one location to another in a given target specimen and a given layer. This suggests that the failure of the hardfaced layer could be caused after considerable plastic deformation of chromium carbides and that the failure can be considered as plastic flow led rupture [24, 25].

Figure 6 shows the microstructural features of location "C" labeled in Fig. 3. In this figure, the deformation of the SS buttering layer is clearly visible (Fig. 6a), being composed of solid-state flow of austenitic buttering layer in between the bullet and BM, as observed by Pizana et al. [25]. The solid-state flow is clearly visible in Fig. 6(b, c). Figure 6 shows the presence of adiabatic shear bands (ASBs). The solid-state flow could be produced when material from the head section near the target–projectile interface is transported. Thus, the shear bands facilitate the high-strain-rate deformation experienced in this region [25].

Figure 7 shows the microstructural features of location "D" labeled in Fig. 3. Figure 7(a) shows the target–bullet interfacial microstructure (where the nose of the bullet was stopped). At the root of the joint, the presence of skeletal δ-ferrite in the austenitic matrix is clearly visible in the micrograph. A part of the hardfaced layer jammed at the interface between the target and projectile is also evident in the same micrograph. In Fig. 7(b), an anomalous pattern of skeletal δ-ferrite in the austenitic matrix in the immediate vicinity of the target–projectile interface is also visible.

Figure 8 shows the microstructural features of location "E" labeled in Fig. 3. This location corresponds to the interface between the hardfacing and SS root layer. The microstructure (Fig. 8a) clearly shows the presence of hanging of buttering layer and hardfaced layer. In Fig. 8(a), the arrow indicates the plausible crack propagation direction starting from the hardfaced layer and propagating toward the soft SS layer. In Fig. 8(b), ASBs are observed, and adjacent to the ASBs, cracks are also seen. Figure 8(a, b)
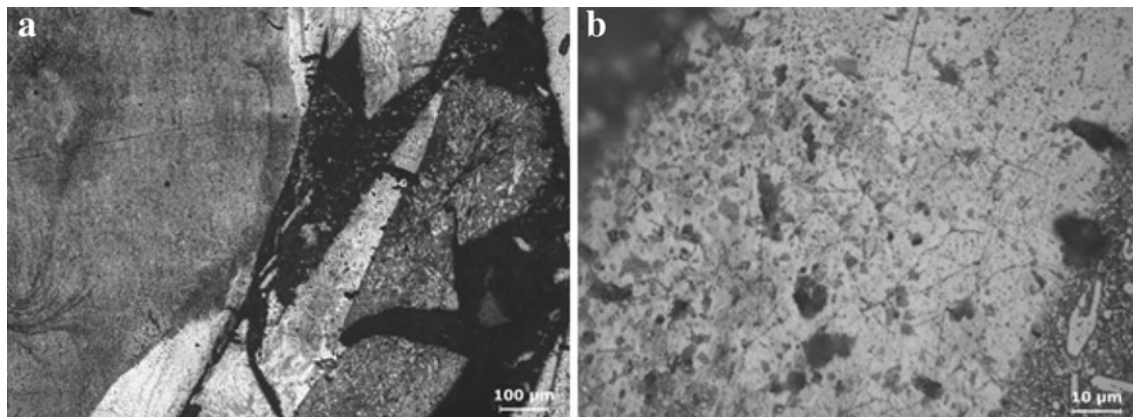

Fig. 3 Microstructure of through-thickness cross section (*arrow* indicates bullet direction)

Fig. 4 Microstructural features of location "A" labeled in Fig. 3 (**a**) at 100× magnification (**b**) at 1000× magnification
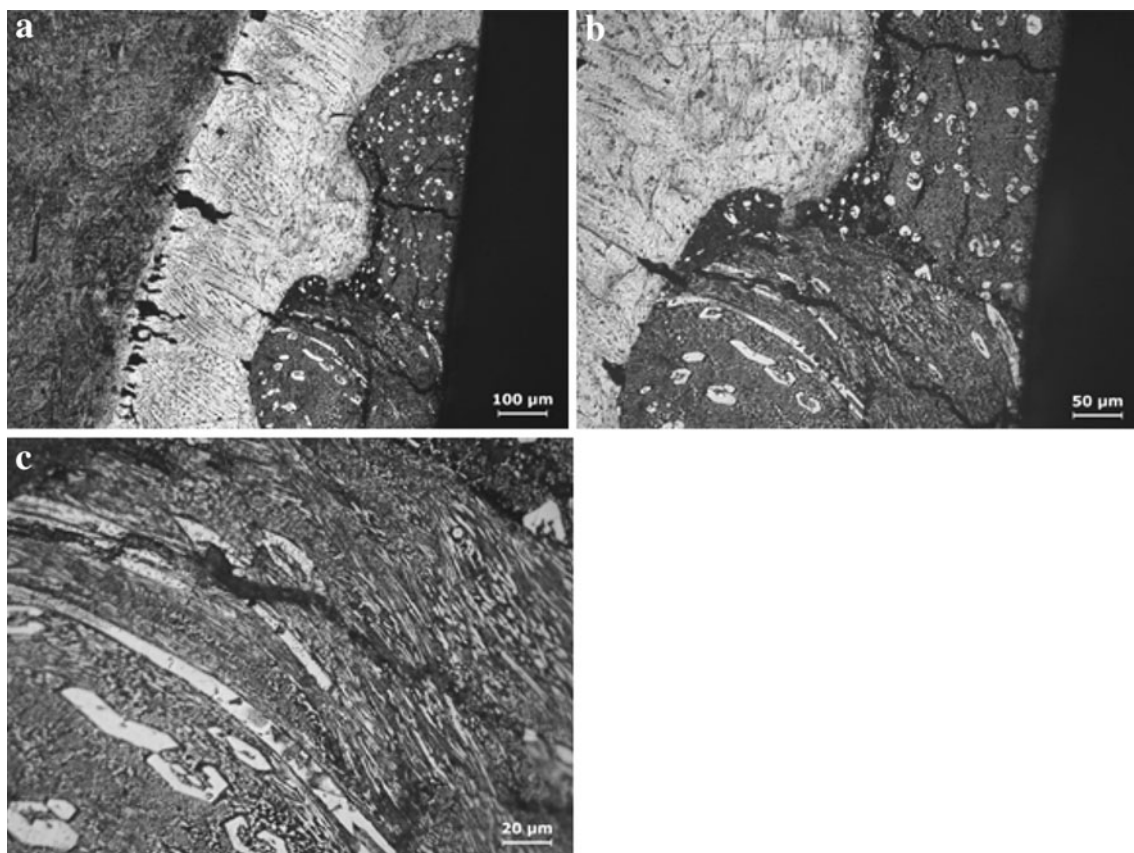
Fig. 5 Microstructural features of location "B" labeled in Fig. 3 (**a**) at 100× magnification (**b**) at 200× magnification (**c**) at 500× magnification

reveals the presence of a crack in both the buttering and the hardfaced layers after ballistic impact. In Fig. 8(c, d), the presence of elongated austenitic grains is clearly visible from the micrographs. This shows that these layers have undergone considerable deformation before crack initiation and separation of layers.

Figure 9 shows the microstructural transformation after ballistic impact at location "F" (different locations of hardfaced region alone) labeled in Fig. 3. From Fig. 9(a, b), it is evident that numerous cracks were generated during the ballistic impact in orientations both parallel and normal to the bullet trajectory. The distribution and shape of the cracks depend on the distance from the impact point. They vary in number from one location to another in a given target specimen and a given layer. However, in Fig. 2(b), it is apparent that no such cracks are presented in the hardfaced layer. This suggests that the cracks are generated during the ballistic impact only.

Figure 10 reveals the microstructural features of location "G" (interface between SS cap and hardfaced region). In Fig. 10(a, b), cracks are present in multiple directions. In Fig. 10(b), crack arrest in the SS capping layer is observed. In Fig. 10(c), the presence of cracking in the interface between the SS capping front layer and hardfaced

interlayer is clearly visible. It is significant that the crack is not in the soft front layer but instead is presented in the hardfaced middle layer in the radial direction (normal to the bullet trajectory). This can be ascribed to the fact that the austenite matrix might have played a role in retarding fast crack propagation as it is a ductile phase. In Fig. 10(c), the needle-like chromium carbides are broken due to the long cracks.

Figure 11 reveals the microstructural features of location "H" labeled in Fig. 3 (the interface between SS capping/buttering layer and hardfaced region). In Fig. 11(a), the interfaces (interface between buttering/hardfacing and hardfacing/SS capping) are clearly visible. The presence of cracks is observed only in the SS capping front layer but not in the SS buttering layer. This can be ascribed to the dilution effect of the SS capping layer with the hardfaced layer and also the impact intensity on the front layer. This impact intensity is comparatively lower in the SS buttering layer, and also the available microstructure in this zone (buttering layer) possesses higher toughness as compared with the chromium carbide microstructure in the hardfaced layer. Figure 11(b–d) depicts a number of microcracks and pull-out of some parts of the hardfaced layer. However, these cracks are completely arrested in the interface
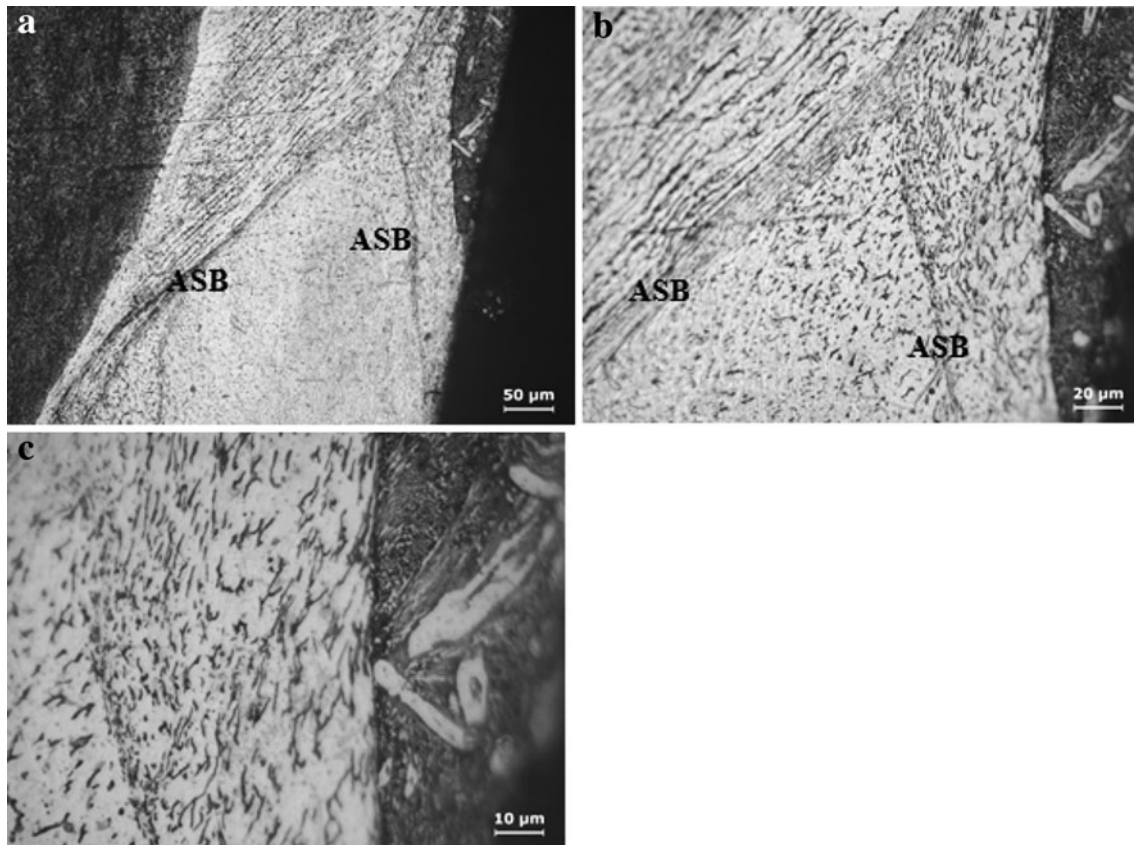
Fig. 6 Microstructural features of location "C" labeled in Fig. 3 (**a**) at 200× magnification (**b**) at 500× magnification (**c**) at 1000× magnification

between the SS buttering layer and hardfacing, because these cracks are blunted by the austenite microstructure.

Hardness

Microhardness measurements were taken along the WCL to identify the hardness profile in the through-thickness direction of the target plate. Similarly, hardness measurements were performed as per the scheme illustrated in Fig. 12(a) to identify the hardness alteration after the ballistic test at three different radial distances from the lip of the unaffected area after projectile travel. For comparative analysis, the hardness profile along the WCL before and after impact is presented in a single graph (Fig. 12c). In this graph, the hardness curve labeled "0 mm" is the hardness profile along the WCL before impact and the hardness profile along 0.4 mm from the lip of the bullet trajectory after impact. Similarly, the hardness curves of 0.1, 0.2, and 0.3 mm are the hardness profiles after ballistic impact at 0.1, 0.2, and 0.3 mm, respectively, from the lip of the bullet trajectory. From these curves, it is observed that a smaller increase in hardness was observed within the localized area (Fig. 12b) that covered with adiabatic shear band as seen in Figs. 6 and 8. A similar increase in

microhardness has been observed by Solberg et al. [26] in the through-thickness direction, irrespective of weld layers. These hardness values are just above the hardness measured in the virgin material (0 mm, hardness along WCL) far from the shear zone.

XRD Results

Comparing the XRD patterns from the two examination locations (Fig. 13), the only difference is the presence of chromium carbide peaks in the section containing both weld metal and BM. The XRD results confirm the presence of austenitic and martensitic peaks in both cases. In addition to the austenitic and martensitic peaks, the presence of Cr_7C_3 and Cr_3C_2 is also confirmed through this XRD analysis in this section. The main peaks of the specimen reveal four phases: face-centered cubic (γ), body-centered cubic (m), hexagonal (Cr_7C_3), and orthorhombic crystal structure (Cr_2C_3). As the hard chromium carbide peaks are observed at high intensity, these results indicate that these phases are more dominant in these layers. The presence of austenitic phases reflects the presence of retained austenite in these regions.
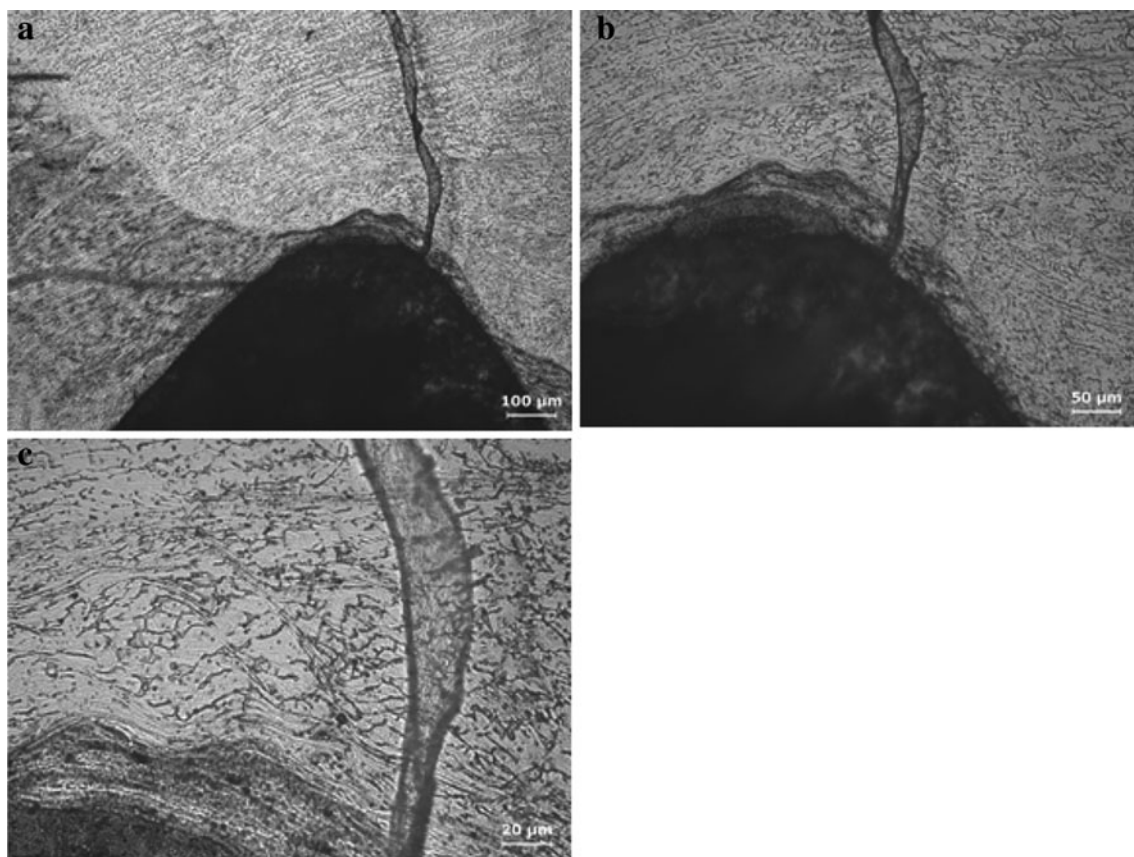
Fig. 7 Microstructural features of location "D" labeled in Fig. 3 (**a**) at 100× magnification (**b**) at 200× magnification (**c**) at 500× magnification

Fracture Surface

The samples exhibit a fibrous fracture surface showing three distinct zones, as shown in Fig. 14. Zones marked 1, 2, and 3 represent the fracture surface of the bulk material and that of the sheared regions, respectively. The transitional deformed band between the bulk material and 1.5 mm depth from the lip of the broken area is shown in zone 2. The appearance of shear bands depended on the distance from the initiation point. Near the edge of the plate in the fractured surface, the shear lips of the broken plate were smooth with very fine dimples. Zone 3 is the large curved surface representing the conical shell of the transformed adiabatic shear band that formed during the combined action of plastic deformation and adiabatic heating along the narrow heat wave paths [12, 13]. Two fracture modes are observed in this zone: ductile shear fracture mode showing highly elongated dimples (Fig. 14b) and knobby fracture mode (Fig. 14c), which suggests partial melting of the grain boundary within the shear bands [27]. This can be ascribed to the high velocity of the projectile; the heat generated in some slip planes does not have enough time to dissipate completely. This local heating prevents homogeneous deformation and thus promotes the

knobby type of fracture mode at this location. The dimples are narrower and more elongated. Both dimpled and knobby fracture occurred along ASB in these specimens, and the transition between ductile shear fracture and knobby fracture modes is clearly visible on the fracture surface.

Discussion

Role of SS Capping in Ballistic Performance Enhancement

In this investigation, it is observed that the fully austenitic weld metal using SS electrode, having a microstructure of δ-ferrite in a plain austenitic matrix, is beneficial for moderate strength welds with good crack resistance. Due to its high alloy content in the SS filler, it can tolerate up to 67 % dilution by the BM without the formation of weld metal martensite. This can be attributed to the low diffusivity of hydrogen in austenite; the fully austenitic weld metal limits the amount of hydrogen diffusivity to the HAZ and consequently reduces the likelihood of HIC [5]. This microstructure can absorb more impact energy due to its
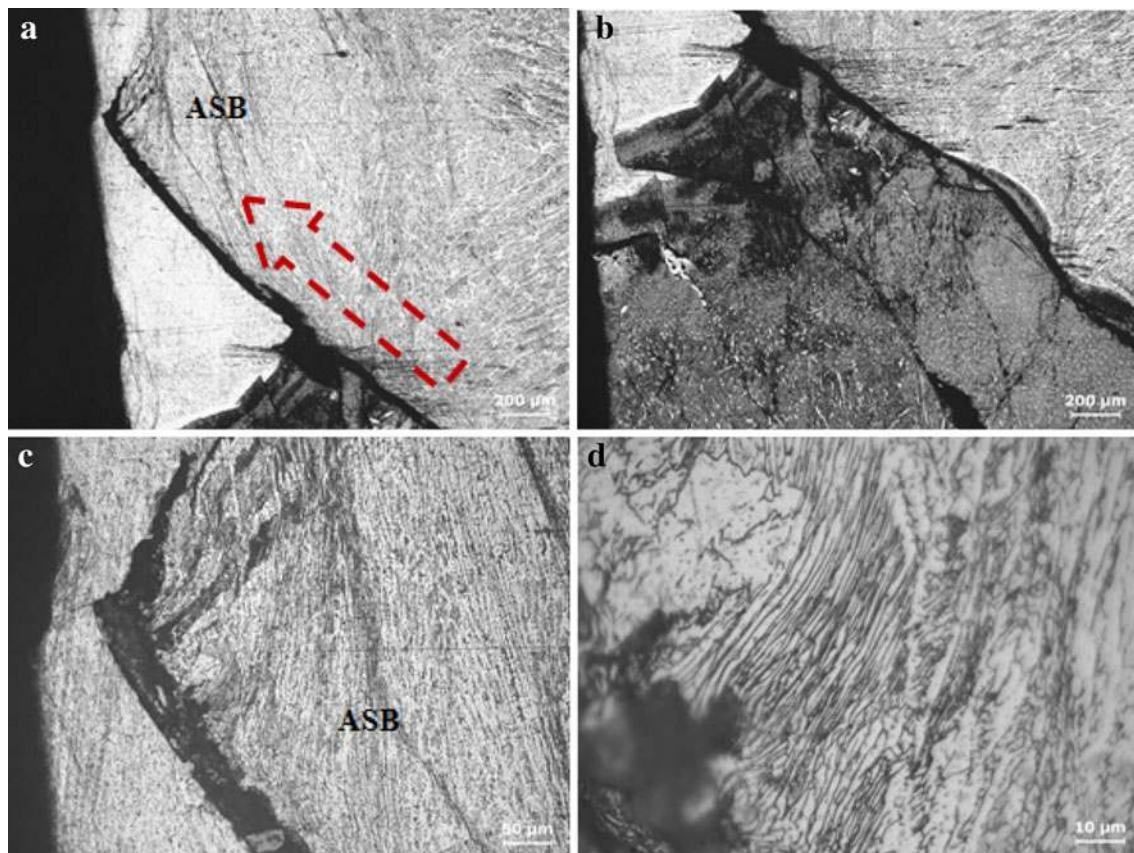
Fig. 8 Microstructural features of location "E" labeled in Fig. 3 (**a**) at 50× magnification (**b**) at 50× magnification (**c**) at 200× magnification (**d**) at 1000× magnification
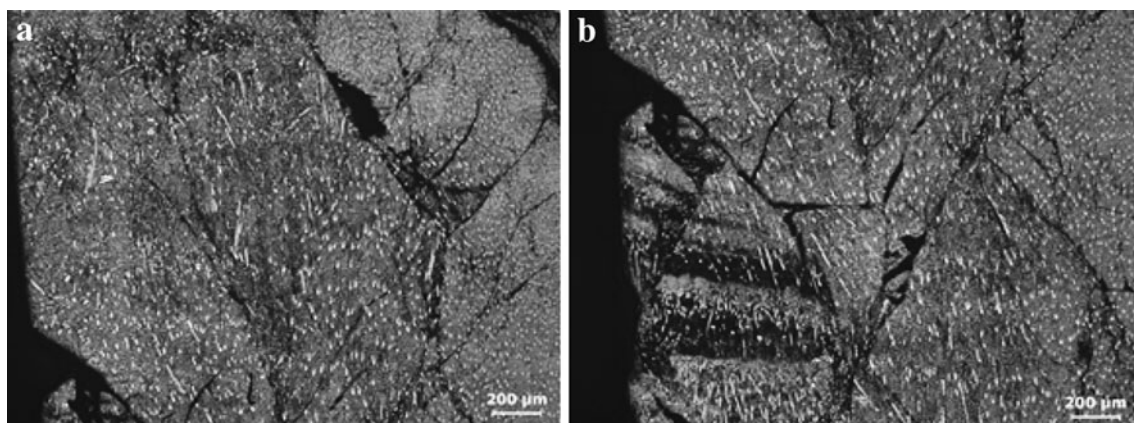

Fig. 9 Microstructural features of location "F" labeled in Fig. 3 (**a**) at 50× magnification (**b**) at 50× magnification

high toughness. The nickel available in these electrodes improves the toughness in two ways. One is by reducing the δ-ferrite content of the weld metal, and the other is by stabilizing the austenite. Thus, the larger austenitic phase along with less δ-ferrite promotes higher toughness [18]. This argument can be confirmed by the results of image analysis of the SS capping. Results indicated 90.5 % austenite and 9.5 % δ-ferrite in the SS capping layer. The

toughness of the austenite is reinforced by the presence of grain boundary δ-ferrite in this capping layer.

Role of Hardfaced Interlayer in Ballistic Performance Enhancement

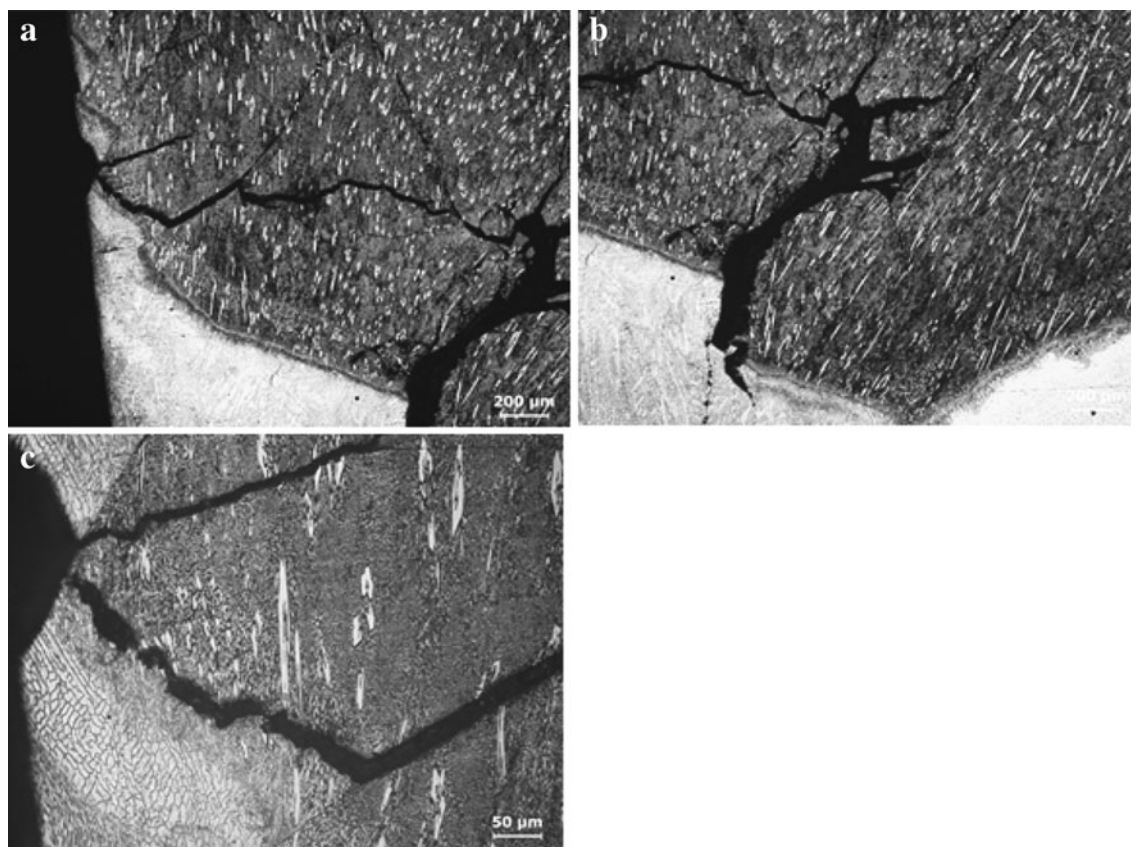Hardfaced weld consisting of uniformly distributed hexagonal chromium carbides in a eutectic austenitic matrix

Fig. 10 Microstructural features of location "G" labeled in Fig. 3 (**a**) at 50× magnification (**b**) at 50× magnification (**c**) at 200× magnification

possessing very high hardness can be beneficial to resist the ballistic impact. XRD analysis confirmed the presence of hexagonal (Cr_7C_3) and orthorhombic crystal structure (Cr_2C_3). The projectile penetration resistance of various armor materials is dependent on their hardness. Adequate toughness is called for, to avoid cracking tendency and consequent disintegration of the material. Generally, the harder the material, the better its resistance to projectile penetration [17, 18]. It was expected that the soft austenitic capping front layer would no longer offer resistance to projectile penetration. The capping front layer allows the bullet to puncture the front layer; when the bullet reaches the hardfaced layers, the hardfacing offers maximum resistance to penetration.

The image analysis results of undiluted hardfaced layer microstructure show the volume fraction of carbides (both hexagonal and needle like) to be 53.5 %, with the remaining 46.5 % being the austenitic matrix. This is beneficial to absorb the maximum ballistic impact and thus reduce the impact velocity of the projectile to zero. The reduction in velocity is effected by cracking of the hardfaced layer in both directions, both transverse and parallel to the bullet trajectory. As the impact energy is intense near the impact point, an aggressive interaction between the

bullet and the target causes a large amount of breakup of the hardfaced layer. The presence of cracks in this region after ballistic testing would be beneficial to stop the bullet penetration by absorbing ballistic impact energy due to cracking of the hardfaced layer and controlling the projectile travel direction to be vertical [23]. In Figs. 5, 10, and 11, the numerous cracks observed in the direction normal to the bullet penetration direction could be attributed to the elements whose tensile strengths are substantially lower than their corresponding compressive values, such as ceramic (chromium carbide hardfaced interlayer) [24].

The gross plastic deformation of the carbide structure can be justified by the presence of austenitic matrix in the hardfaced layer, as discussed for the weld metal undiluted hardfaced microstructure (Fig. 2b). The existence of microvoids at the interface between the buttering layer and hardfaced layer in Fig. 6(d) reflects the competence of the joint at the time of impact. This could be explained if the joint reliability were poor, so these layers might have disintegrated after impact. However, here this was not the case. This suggests that the ballistic resistance of the welded joint is improved by the presence of the hardfaced interlayer, which is supported by the presence of the soft
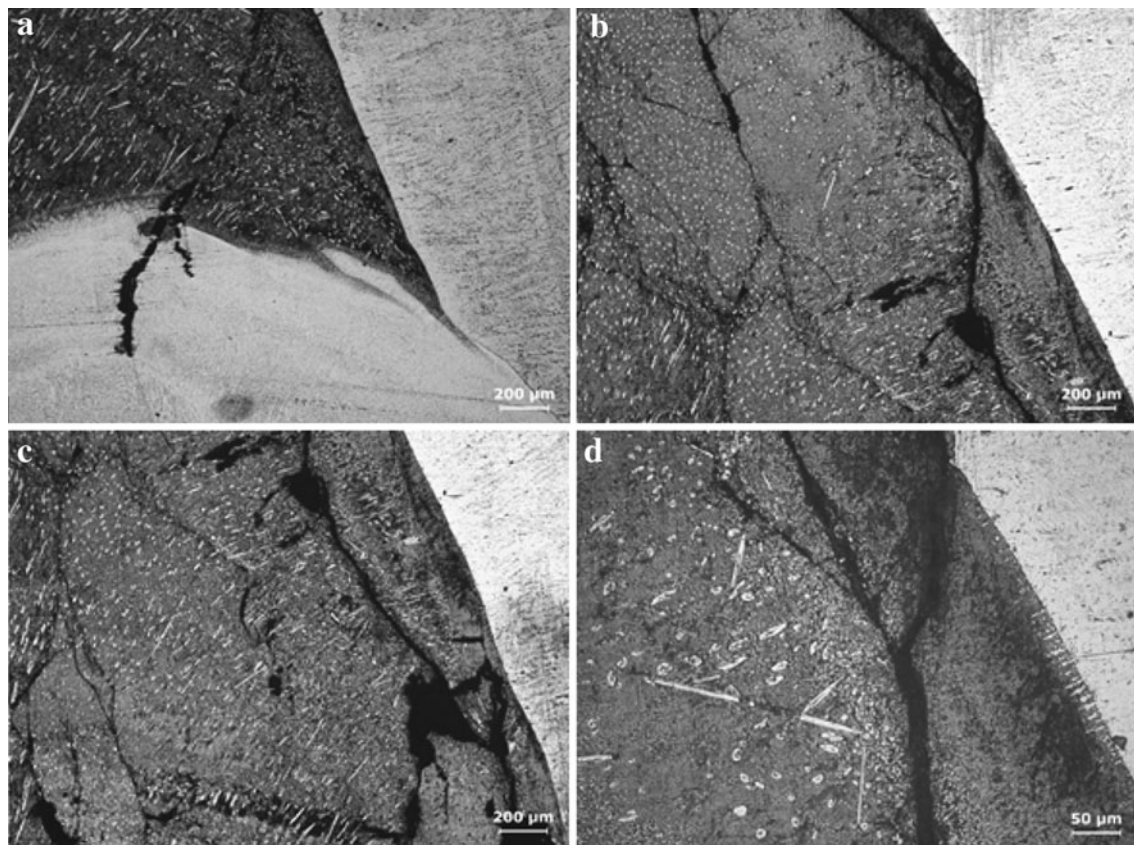
Fig. 11 Microstructural features of location "H" labeled in Fig. 3 (**a**) at 50× magnification (**b**) at 50× magnification (**c**) at 50× magnification (**d**) at 200× magnification

and tough austenitic SS buttering layer. This is because the projectile retains its path through the soft layer and then hits the hard layer in the center, thereby resulting in more efficient retention of the projectile travel and less crack formation. In addition, the soft SS layer is beneficial in producing the crack-free new surface of the hardfaced region through melting and subsequent solidification during welding of the SS layer. This cures the cracks produced during hardfacing of the high-chromium-carbide interlayer. The elongated chromium carbide structure in both hexagonal and plate-like chromium carbide is clearly visible in Fig. 5(b, c). This is attributed to the energy absorption, which is primarily achieved by the hardfaced layer through the generation of numerous cracks in both the longitudinal and transverse directions. The hard layer of high-carbon, high-chromium alloy absorbs the ballistic impact energy by forming a high density of cracks [23].

Role of SS Root in Ballistic Performance Enhancement

Image analysis results of SS root revealed that ferrite accounted for approximately 16.8 %, with the balance (83.2 %) being austenite. Here, the grain boundary δ-ferrite in the plain austenitic matrix present in the SS capping is

changed into dispersed δ-ferrite in a massive austenitic matrix. This could be due to the successive heat supplied by the deposition of hardfacing and capping layer. Due to the longer cooling time, the plain austenitic matrix is changed into massive austenite and also the δ-ferrite present in the grain boundaries of austenite is dispersed into the massive austenite and exhibits a vermicular morphology. Image analysis results indicate that there is a small amount of reduction of δ-ferrite as compared with the SS capping layer due to the longer cooling time supplied by the successive weld deposits. This is also beneficial to improve the impact toughness of the root layer due to the presence of an increased amount of austenite. Figure 7 shows the location corresponding to the sharp-nosed projectile–target interface. Here, the amount of distorted microstructure is less as compared with the other locations. This could be ascribed to the total impact energy being completely absorbed by the multilayered target before the projectile reaches this DOP. A small amount of solid-state flow in the immediate vicinity of the target–bullet interface is also observed in Fig. 7(c). This indicates that the layer present at the root side after the bullet penetrates to DOP of about 14 mm is sufficient to completely stop the bullet from further progression into the target. This is possible

Fig. 12 Hardness test results. (a) Macrostructure of the joint before impact. (b) Microstructure of the joint after impact and schematic illustration of hardness measurement map. (c) Hardness profile along the weld center line at different locations of the joint before and after impact
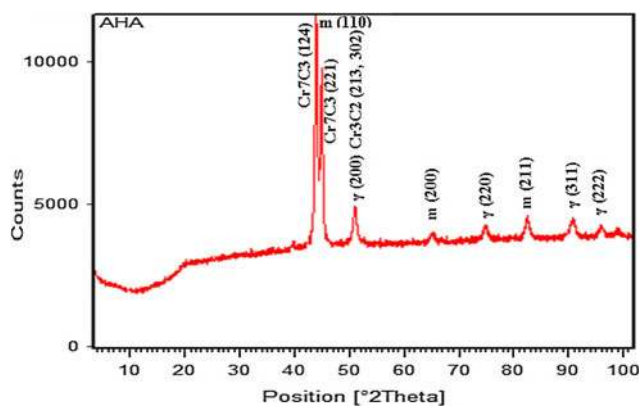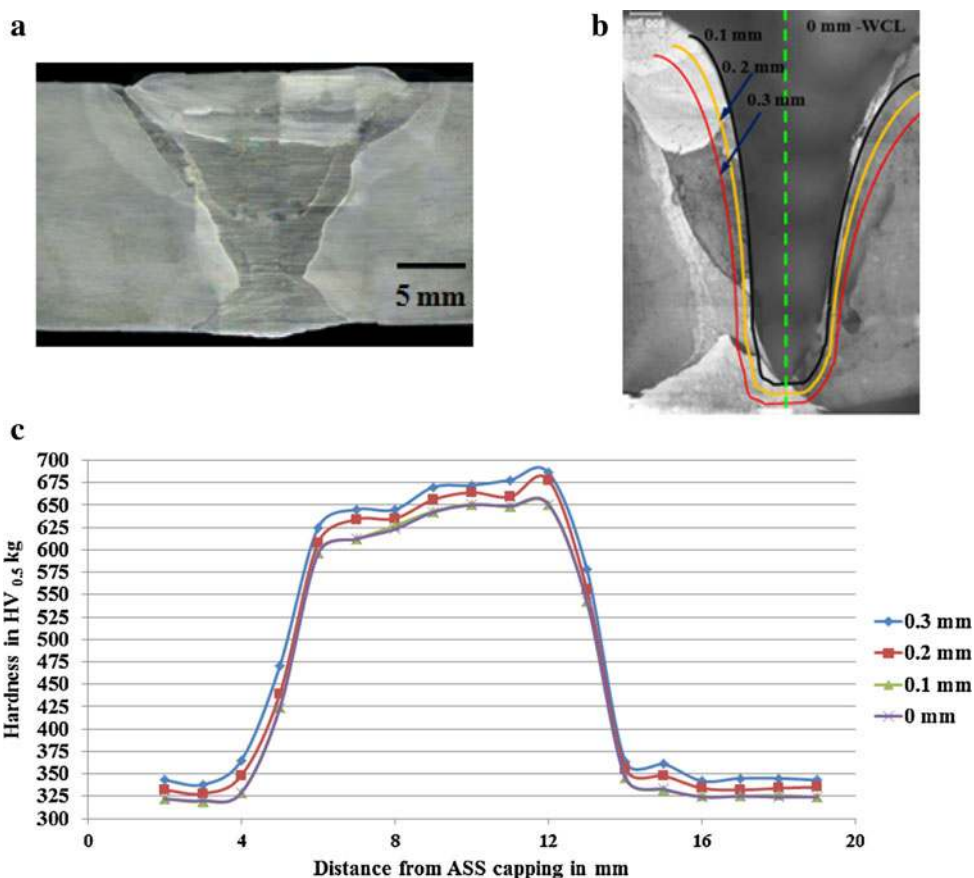

Fig. 13 XRD pattern for weld metal/base metal

only because of the presence of the capping front layer and hardfaced middle layer, because the maximum available impact energy is reduced when the bullet crosses these layers is believed to be more. The remaining energy available at the bullet–target interface is minuscule and is not sufficient to cause any further penetration. Thus, it causes only a small amount of solid-state flow in the immediate vicinity of the target–bullet interface. This is the reason for the presence of a lesser amount of distorted microstructure in the immediate vicinity of the target–

bullet interface (Fig. 7c), while the other locations possess strongly distorted microstructure (Figs. 6, 7). Again the absence of adiabatic shear band in this region in Fig. 7 can be ascribed to this lower available impact energy reduced by the other (SS capping front and hardfacing) layers.

Role of SS Buttering Layer in Ballistic Performance Enhancement

From Fig. 6, it is very clear that, at the time of bullet travel through the weld layers, there is a considerable amount of plastic flow of weld metal. A schematic illustration of the material flow is presented in Fig. 15. The material flow in this case is outward, opposite to the bullet direction, and perpendicular to the target surface because of the presence of very high-hardness BM next to the soft SS buttering layer; this could be the reason for the arrest of the material flow in the direction perpendicular to the bullet penetration and parallel to the target surface. The highly distorted grain boundary δ-ferrite is clearly visible in Fig. 6(b, c). This shows the capability of the austenite matrix present in the buttering layer against the high-strain-rate deformation, which is assisted by the distortion of δ-ferrite present in the grain boundaries of this layer. Though solid-state material flow occurred in the adjacent region (SS buttering layer),
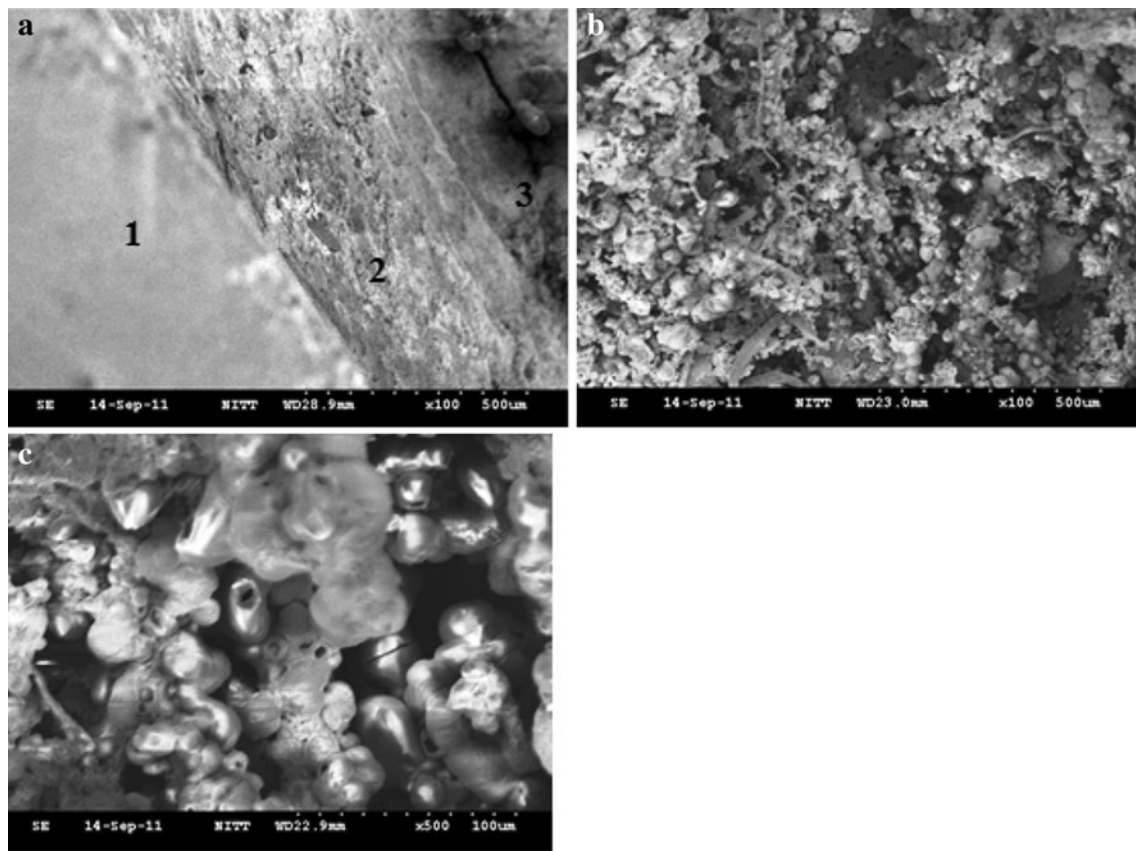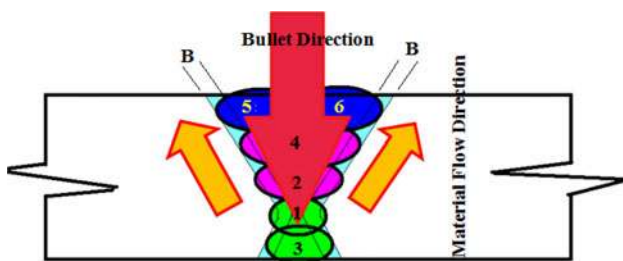
Fig. 14 Fracture surface of bullet path

Fig. 15 Schematic illustration shows the probable solid state flow of material at the time of impact (1–6 sequence of deposition; layers 1, 3, 5 & 6 represents the ASS weld, layers 2 and 4 are hardfacing and 'B' is ASS buttering layer.)

there is no evidence of separation of the buttering layer and hardfacing layer (Figs. 5b, 6(b, c)). These results again exemplify the joint integrity between these two layers after the ballistic impact. The highly distorted microstructure of δ-ferrite in a plain austenite matrix is clearly visible in Fig. 6(f). The presence of massive austenite and dispersed δ-ferrite in the austenitic matrix is clearly visible instead of the grain boundary δ-ferrite present in the austenitic matrix as seen in Fig. 2(b). This could be attributed to the solid-state material flow of the austenitic buttering layer in between the bullet and BM. This microstructure appears like that of a dispersion-strengthened composite. These microstructural changes could be the reason for the maximum impact energy absorbed by the massive austenite, toughened by the dispersed δ-ferrite in the massive austenite matrix, during the ballistic impact [28]. The buttering layer provides high joint integrity by keeping the hardness level in between the BM hardness and weld metal hardness. The interface microstructure and microhardness play a critical role in keeping the joint more stable at the time of projectile impact. The microstructure between the buttering layer and the BM shows a clear anchoring between these two dissimilar metals, having a hardness value between 255 and 445 $HV_{0.5}$. Due to this level of hardness, joint disintegration is prevented during projectile impact.

Effect of Ballistic Impact on Hardness

The hardness is markedly increased within the localized area (Fig. 12) that covered with adiabatic shear band as seen in Figs. 6 and 8. A similar increase in microhardness was observed by Solberg et al. [26] in the through-thickness direction, irrespective of weld layers. These hardness values are just above the hardness measured in the virgin material (0 mm, hardness along WCL) far from the shear

zone. This indicates that there is no possible phase transformation, and the increase in hardness could be due to deformation-induced microstructure changes (Figs. 5–11) and work-hardening effect [28]. Even though no microstructural changes were discovered for undiluted hardfaced layers, a small increase in hardness was detected due to the deformation-induced hardening of this zone by the ballistic impact. Even these zones before impact possess a very high hardness, resulting in the generation of numerous cracks in both directions. This prevents adiabatic shear band formation in this zone.

Role of Sandwiched Joint Design in Ballistic Performance Enhancement

Sandwiching of the hardfacing alloy weld between SS weld layers improves the ballistic resistance by way of a possible reduction of the projectile velocity coupled with crack blending behavior. When the projectile hits the hard layer directly, it proceeds off-beam and tends to produce more cracks in the hard layer. This might lead to subsequent fragmentation and separation from the substrate. However, when the soft layer is welded over the hard layer, the overall ballistic property of the hardfaced specimen would be improved. This is because the projectile retains its trajectory through the soft layer and then hits the hard layer in the interior, thereby resulting in more efficient restraint of the projectile travel and reduction of crack formation. In addition, the soft layer is advantageous in producing the crack-free new surface of the hardfaced specimen through melting and subsequent solidification during welding of the SS layer, thereby curing cracks produced during hardfacing of the chromium carbide interlayer. The combination of hard and soft layers is the reason for the enhancement of the ballistic resistance through absorption of ballistic impact energy by cracking of primary carbides in the hardfaced layer and controlling the projectile travelling direction as vertical due to the presence of the soft backing layer.

Conclusions

An attempt was made to exemplify the microstructural transformations that occur in a ballistically tested multi-layered armor steel joint. Results show that:

1. The sandwiched joint fabricated with a 5.5-mm chromium carbide hardfaced interlayer on both sides of the SS layer showed improved ballistic performance over the BM with a DOP of 14 mm.
2. The hard layer containing chromium carbide absorbs the ballistic impact energy by forming high-density cracks.
3. The combination of hard and soft layers improved the ballistic immunity of the joint by absorbing impact energy (due to cracking of primary carbides) and controlling the projectile travelling direction as vertical due to the presence of the soft backing layer by way of possible reduction of projectile velocity coupled with crack blunting behavior.
4. The buttering layer enhances ballistic immunity by the resultant microstructure and hardness distribution and successfully keeps the weld layers intact when the projectile is fired at the WCL, interfaces, and HAZ.
5. At the WCL, further investigation is required for analytical correlation of the projectile shattering mechanism and resulting hardness distribution, because this study correlated the ballistic test results with the resultant microstructure and microhardness values.

References

1. F. Ade, Ballistic qualification of armour steel weldments. Weld. J. **70**, 53–56 (1991)
2. G. Madhusudhan Reddy, T. Mohandas, Ballistic performance of high-strength low-alloy steel weldments. J. Mater. Process. Technol. **57**, 23–30 (1996)
3. G. Madhusudhan Reddy, T. Mohandas, G.R.N. Tagore, Weldability studies of high-strength low-alloy steel using austenitic fillers. J. Mater. Process. Technol. **49**, 213–228 (1995)
4. S.J. Alkemade, The weld cracking susceptibility of high hardness armour steel. Defense Science and Technology Organization, Australia, 1996; AR No: 009-659: 1–17
5. G. Magudeeswaran, V. Balasubramanian, G. Madhusudhan Reddy, Hydrogen induced cold cracking studies on armour grade high strength, quenched and tempered steel weldments. Int. J. Hydrogen Energy **33**, 1897–1908 (2008)
6. G. Madhusudhan Reddy, T. Mohandas, D.S. Sarma, Cold cracking studies on low alloy steel weldments: effect of filler metal composition. Sci. Technol. Weld. Join. **8**(6), 407–414 (2003)
7. G. Madhusudhan Reddy, T. Mohandas, K.K. Papukutty, Effect of welding process on the ballistic performance of high-strength low-alloy steel weldments. J. Mater. Process. Technol. **74**, 27–35 (1998)
8. G. Madhusudhan Reddy, T. Mohandas, K.K. Papukutty, Enhancement of ballistic capabilities of soft welds through hardfacing. Int. J. Impact Eng. **22**, 775–791 (1999)
9. T. Mohandas, G. Madhusudan Reddy, B. Satish Kumar, Heat-affected zone softening in high-strength low-alloy steels. J. Mater. Process. Technol. **88**, 284–294 (1999)
10. P.K. Jena, K. Ramanjeneyulu, K. Siva Kumar, T. Balakrishna Bhat, Ballistic studies on layered structures. Mater. Des. **30**(6), 1922–1929 (2009)

11. M. Balakrishnan, V. Balasubramanian, G. Madhusudhan Reddy, K. Sivakumar, Effect of buttering and hardfacing on ballistic performance of shielded metal arc welded armour steel joints. Mater. Des. **32**, 469–479 (2011)

12. M. Balakrishnan, V. Balasubramanian, G. Madhusudhan Reddy, K. Sivakumar, Effect of hardfaced interlayer thickness on ballistic performance of armour steel welds. Mater. Des. **44**, 59–68 (2013)

13. A.G. Odeshi, M.N. Bassim, High strain-rate fracture and failure of a high strength low alloy steel in compression. Mater. Sci. Eng. A **525**, 96–101 (2009)

14. K. Maweja, W. Stumpf, Fracture and ballistic-induced phase transformation in tempered martensitic low-carbon armour steels. Mater. Sci. Eng. A **432**, 158–169 (2006)

15. S. Deya, T. Børvik, O.S. Hopperstad, J.R. Leinum, M. Langseth, The effect of target strength on the perforation of steel plates using three different projectile nose shapes. Int. J. Impact Eng. **30**, 1005–1038 (2004)

16. Y.V. Milman, S.I. Chugunova, I.V. Goncharova, V.A. Goncharuk, N.A. Yefimov, Physics of deformation and fracture at impact loading and Penetration. Int. J. Impact Eng. **33**, 452–462 (2006)

17. L.E. Murr, E.T. Ferreyra, S. Papu, E.P. Garcia, J.C. Sanchez, W. Huang, J.M. Rivas, C. Kennedy, A. Ayaa, C.S. Niou, Novel deformation processes and microstructures involving ballistic penetrator formation and hypervelocity impact and penetration phenomena. Mater. Charact. **37**, 245–276 (1996)

18. G. Magudeeswaran, V. Balasubramanian, T.S. Balasubramanian, G. Madhusudhan Reddy, Effect of welding processes and consumables on tensile and impact properties of high strength quenched and tempered steel joint. J. Iron Steel Res. **15**(6), 87–94 (2008)

19. ASTM E-384-05, Standard test method for micro indentation hardness of materials (2005)

20. P.K. Jena, K. Siva Kumar, V. Rama Krishna, A.K. Singh, T. Balakrishna Bhat, Studies on the role of microstructure on performance of a high strength armour steel. Eng. Fail. Anal. **15**, 1088–1096 (2008)

21. ASME Boiler and pressure vessel code, Sec II part-C: specification for welding rods, filler metals and electrodes. SFA 5.13, Specification for surfacing electrodes for shielded metal arc welding (The American Society of Mechanical Engineers New York, 2004), pp. 303–324

22. S.J. Unfried, C.M. Garz'onb, J.E.J. Giraldoc, Numerical and experimental analysis of microstructure evolution during arc welding in armor plate steels. Mater. Process. Technol. **209**, 1688–1700 (2009)

23. S.-H. Choo, E.-R. Baek, S. Lee, Ballistic impact behaviour of multilayered armor plates processed by hardfacing. Metall. Mater. Trans. A **27A**, 3335–3340 (1996)

24. M.E. Backman, W. Goldsmith, The mechanics of penetration of projectiles into targets. Int. J. Eng. Sci. **16**, 1–99 (1978)

25. C. Pizana, L.E. Murr, M.T. Baquera, I.A. Anchondo, A. Putrevu, C.Y. Pina, T.C. Tamoria, H.C. Chen, S.J. Cytron, Solid-state flow, mechanical alloying, and melt-related phenomena for [0 0 1] single-crystal W ballistic rod penetrators interacting with steel targets. Mater. Sci. Eng. A **428**, 301–313 (2006)

26. J.K. Solberg, J.R. Leinum, J.D. Embury, S. Dey, T. Børvik, O.S. Hopperstad, Localised shear banding in Weldox steel plates impacted by projectiles. Mech. Mater. **39**, 865–880 (2007)

27. H. Berns, S. Riedner, V. Gavriljuk, Y. Petrov, A. Weihrauch, Microstructural changes in high interstitial stainless austenitic steels due to ballistic impact. Mater. Sci. Eng. A **528**, 4669–4675 (2011)

28. B.V. Cockeram, Some observations of the influence of δ-ferrite content on the hardness, galling resistance, and fracture toughness of selected commercially available iron-based hardfacing alloys. Metall. Mater. Trans. A **33A**, 3403–3419 (2002)